UC Davis
UC Davis Previously Published Works

Title
A computational and experimental study of thermal energy separation by swirl

Permalink
https://escholarship.org/uc/item/7q07f163

Authors
Kobiela, B
Younis, BA
Weigand, B
et al.

Publication Date
2018-09-01

DOI
10.1016/j.ijheatmasstransfer.2018.03.058

Peer reviewed

eScholarship.org Powered by the California Digital Library
University of California

International Journal of Heat and Mass Transfer 124 (2018) 11–19

Contents lists available at ScienceDirect

International Journal of Heat and Mass Transfer

journal homepage: www.elsevier.com/locate/ijhmt

A computational and experimental study of thermal energy separation by swirl

B. Kobiela [a], B.A. Younis [b,*], B. Weigand [a], O. Neumann [c]

[a] Institut für Thermodynamik der Luft- und Raumfahrt, Universität Stuttgart, 70569 Stuttgart, Germany
[b] Department of Civil & Environmental Engineering, University of California, Davis, CA 95616, USA
[c] Department of Mechanical Engineering, University of Applied Sciences, 24149 Kiel, Germany

ARTICLE INFO

Article history:
Received 22 December 2017
Received in revised form 14 March 2018
Accepted 16 March 2018
Available online 21 March 2018

Keywords:
Energy separation by swirl
Turbulent heat fluxes
Ranque-Hilsch effect

ABSTRACT

When compressed air is introduced into a tube in such a way as to generate a strong axial vortex, an interesting phenomenon is observed wherein the fluid temperature at the vortex core drops below the inlet value, while in the outer part of the vortex, the temperature is higher than at inlet. The most familiar manifestation of this phenomenon is known as the Ranque-Hilsch effect, and several alternative explanations for it have been proposed. In this study, we present an analysis of the heat transfer mechanism underlying this phenomenon, based on consideration of the exact equation governing the conservation of the turbulent heat fluxes. The outcome is a model that explicitly accounts for the dependence of the heat fluxes on the mean rates of strain, and on the gradients of mean pressure. These dependencies, which are absent from conventional closures, are required by the exact equation. To verify the model, an experimental investigation of flow in a swirl chamber was conducted, and the measurements were used to check the model's performance as obtained by three-dimensional numerical simulations. Comparisons between predictions and measurements demonstrate that the new model yields predictions that are distinctly better than those obtained using conventional closures.

© 2018 Elsevier Ltd. All rights reserved.

1. Introduction

Vortices that influence the local temperature distribution are frequently encountered in nature and in engineering practice. In the core of a strong vortex, for example, the static temperature is significantly lower than the ambient temperature. It is for this reason that water vapour condenses in the funnel of a tornado, and in the core of the wing tip vortex of an aircraft landing in humid air. An extreme manifestation of the effect of vortical motion on local temperature is seen when compressed air is introduced into a circular tube via tangential inlet slots designed to induce a strong axial vortex. Measurements show that in the core of the vortex, the temperature (both static and total) drops to a value lower than that at inlet, while in the outer part of the vortex, it is higher. The most familiar manifestation of this phenomenon of "thermal energy separation" is the Ranque-Hilsch effect (Fig. 1). Another manifestation, which is the subject of this study, is the flow in a swirl chamber where in the absence of a cold-air outlet, the temperature separation is evident in a substantial decrease of temperature at the vortex axis relative to the inlet value.

Several alternative explanations of the Ranque-Hilsch effect have been put forward since the phenomenon was first observed by Ranque [1] and elaborated on further by Hilsch [2]. A thorough review of the literature on this subject can be found in Eiamsaard and Promvonge [3]. Behera et al. [4], for example, assumed that the mechanism is related to viscous shear that arises due to the strong radial variation of the circumferential velocity. Kurosaka [5] attributed the effect to "acoustic streaming". When flow occurred in a vortex tube with an open outlet, measurements showed that the temperature in the vortex core was lowered, vortex breakdown occurred and pressure fluctuations with descent frequencies. When the pressure fluctuations were suppressed by using Helmholz resonators, the temperature in the vortex core increased and the vortex breakdown did not occur. Gutsol [6] assumed that there is a "sorting" of fluid particles with different speeds and therefore energy separation occurred due to centrifugal forces, i.e. faster particles move radially outwards. Eckert [7] explained the temperature change by adiabatic compression processes. The uncertainty regarding the mechanism underlying this phenomenon is not diminished by recent experimental findings. Thus, while the phenomenon is clearly evident when the working fluid is air [8–10], the situation is far less clear when the working fluid is water. Balmer [11], for example, in experiments in water, showed that a

* Corresponding author.
E-mail address: bayounis@ucdavis.edu (B.A. Younis).

https://doi.org/10.1016/j.ijheatmasstransfer.2018.03.058
0017-9310/© 2018 Elsevier Ltd. All rights reserved.

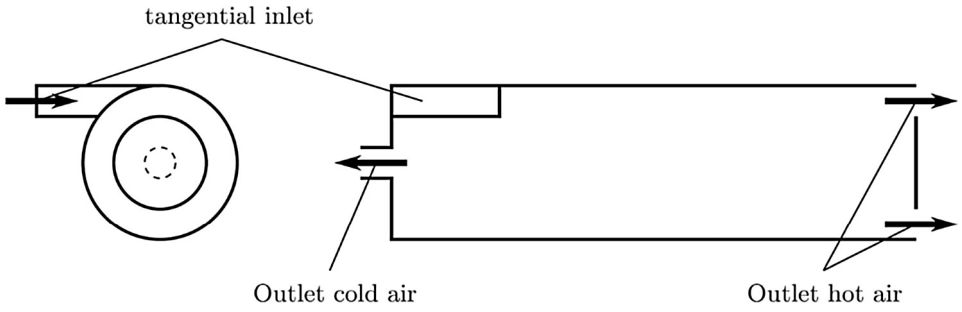

Fig. 1. Schematic view of a Ranque-Hilsch tube.

temperature separation can still be observed, but the static temperature of the cold water at outlet was higher than that at inlet. Clearly compressibility effects that will have been absent from the water experiments will have played a more important role than hitherto suspected. This is confirmed in the study of Polihronov and Straatman [12] who considered the simplified but related case of the radial flow of a compressible fluid taking place in a uniformly rotating adiabatic duct. From consideration of the equation governing the conservation of energy in a rotating fluid under adiabatic conditions, they derive an expression for the total temperature that shows this quantity to depend on both the axial and angular velocities and hence vary in the radial direction leading to temperature separation. Their analysis highlighted the important role of compressibility in the process of temperature separation since, in its absence, the fluid cannot give away internal energy and hence cooling cannot take place.

The numerical simulation of flows in which thermal energy separation as manifested by the Ranque-Hilsch effect has also received much attention and comprehensive reviews of previous work in this area can be found in [13,14]. Farouk and Farouk [15] reported results obtained with Large-Eddy Simulations that showed that, while the flow field was well predicted, the total temperature separation at the cold exit underpredicted the measurements. Most other previous numerical studies of the thermal energy separation as manifested by the Ranque-Hilsch effect have been based on the solution of the Reynolds-averaged form of the equations governing the conservation of mass, momentum and energy [3,4,9]. In this approach, closure models are needed to approximate the unknown turbulence correlations that arise from the averaging process. While a variety of different models were used to obtain the Reynolds stresses, the turbulent heat fluxes were invariably modelled by using Fick's law in which the turbulent diffusivity was defined on the basis of a constant turbulent Prandtl number. The outcomes were generally the same: the predicted difference in total temperature was always smaller than that observed in experiments. Moreover, the calculated profile of static temperature exhibited a maxima on the tube axis and thereafter a decrease towards the adiabatic tube wall. This is contrary to the measured behaviour where the static temperature at the tube axis was in fact at minima. Taken together, these results strongly suggest that the simple model for the turbulent heat flux is not adequate in this case. In the study of Polihronov and Straatman [12] mentioned earlier, computations were performed of the flow in a rotating rectangular duct with adiabatic walls with heated flow introduced at the inlet. Comparisons of the temperature drop between inlet and outlet as computed with their theoretical model with results obtained from solving the conservation equations in three dimensions showed very close agreement between the two. The authors point out a number of important differences between the rotating duct flow considered, and the more complex flow in a vortex tube notably in the necessity of a hot fluid outlet in the vortex tube flow and the absence of such an outlet in the rotating duct case. The patterns of thermal energy transfer, being partly dependent on turbulent diffusion, wil thus be different in the two cases and hence the need for further computations to demonstrate the utility of the theoretical model in a vortex tube flow.

In this paper, we put forward an explanation for the thermal energy separation by swirl based on analysis of the fundamental equations governing conservation of momentum and thermal energy in vortical flows. It will be shown that the phenomenon can be explained from consideration of the thermal energy transport associated with the turbulent heat flux and the turbulent volume work in a pressure gradient field in a compressible fluid. A model for the turbulent heat fluxes that can account for these effects is proposed, and its validity is checked by comparisons with experimental data obtained in a swirl chamber.

2. Analysis and model development

The exact equations that govern the conservation of the turbulent heat fluxes in compressible flows are obtained from the Navier-Stokes and energy equations by replacing the instantaneous variables by the sum of mean and fluctuating parts, and by time-averaging after some manipulation. Le Ribault and Friedrich [16] give the outcome as:

$$\begin{aligned} c_p\frac{\partial\rho\overline{u_i t}}{\partial\tau}+c_p\frac{\partial\rho U_j\overline{u_i t}}{\partial x_j} &= -\rho c_p\overline{u_j t}\frac{\partial U_i}{\partial x_j}-\rho c_p\overline{u_i u_j}\frac{\partial T}{\partial x_j} \\ &\quad -c_p\frac{\partial}{\partial x_j}(\rho\overline{u_i u_j t}+\overline{pt}\delta_{ij})+\overline{\tau_{jk}u_i}\frac{\partial u_k}{\partial x_j}+c_p\overline{t\frac{\partial\tau_{ij}}{\partial x_j}} \\ &\quad -\overline{u_i\frac{\partial q_j}{\partial x_j}}+\overbrace{\overline{u_i\frac{\partial p}{\partial\tau}}+U_j\overline{u_i\frac{\partial p}{\partial x_j}}+\overline{u_iu_j}\frac{\partial P}{\partial x_j}+\overline{u_iu_j\frac{\partial p}{\partial x_j}}}^{} \end{aligned} \tag{1}$$

where U, T and P are the mean components of velocity, temperature and pressure, respectively, u, t and p are their fluctuating values, ρ is the density, c_p is the heat capacity at constant pressure, $\tau_{ij}(=\mu(\partial u_i/\partial x_j+\partial u_j/\partial x_i)-2/3\mu(\partial u_k/\partial x_k)\delta_{ij})$ is the stress tensor with μ being the dynamic viscosity and $q_j(=-\lambda\partial T/\partial x_j)$ is Fourier's heat-flux vector with λ being the molecular diffusivity [16].

While Eq. (1) can be used to obtain the turbulent heat fluxes after the unknown correlations that appear there have been suitably modeled, it would be more convenient from a practical standpoint to use this equation to derive an algebraic model that is simpler to implement in a computational procedure yet one that contains all the requisite dependencies to represent the effects of compressibility, turbulence, and the mean rates of strain. In this regard, attention is drawn to the group of terms that appear on the last line of Eq. (1). These terms, which originate from expansion of $\overline{u_iD(P+p)/D\tau}$, represent the contribution to the turbulent scalar

fluxes due to the work done by the pressure field. In formulating the heat-flux model, it is important to note that the term in that group that contains the mean pressure gradient does not also contain gradients of temperature or of mean velocity. This suggests that for the algebraic model to accurately reflect the contributions made by these terms, it should be formulated in the form:

$$-\rho\overline{u_i t} = D_{Tij}\frac{\partial T}{\partial x_j} + D_{p_{ij}}\frac{\partial P}{\partial x_j} \tag{2}$$

where D_{Tij} is the turbulent diffusivity tensor [17] which is unknown and in need of approximation, and $D_{p_{ij}}$ is a second-order tensor that is a function of the Reynolds-stress tensor and the turbulence time scale but not a function of the velocity or temperature gradients. In this work, and following usual practice, this time scale is assumed to be proportional to the ratio k/ϵ i.e. of the turbulence kinetic energy to its rate of dissipation by viscous action.

Several proposals for modelling D_{Tij} can be found in the literature. In this study, we adopt the proposal of Younis et al. [19] who used tensor representation to obtain an explicit expression for $\overline{u_i t}$ in terms of the vector and tensor quantities suggested by Eq. (1). When the mean pressure gradient is finite, the following functional relationship is obtained:

$$-\overline{u_i t} = f_i\left(\overline{u_i u_j}, \frac{\partial U_i}{\partial x_j}, \frac{\partial T}{\partial x_j}, \frac{\partial P}{\partial x_j}\right) \tag{3}$$

Smith [18] gives the general representation for $\overline{u_i t}$, a first-order tensor, in terms of the first- and second-order tensors in the functional relationship of Eq. (3). This representation and the assumptions underlying its simplification for the case with no pressure gradients are given in [19] and hence will not be reproduced here. When the gradients of mean pressure are finite, additional terms arise. If the terms that involve the products of two second-order tensors are dropped (which is in keeping with the approximations of the previous study), the following pressure-gradient related terms remain:

$$\alpha_1\frac{\partial P}{\partial x_i}, \quad \alpha_2\overline{u_i u_j}\frac{\partial P}{\partial x_j}, \quad \alpha_3\frac{\partial U_i}{\partial x_j}\frac{\partial P}{\partial x_j}, \quad \alpha_4\frac{\partial T}{\partial x_j}\frac{\partial P}{\partial x_j}$$

where the αs are linear multipliers that are required for dimensional consistency.

It is immediately evident that only one of the terms in this representation corresponds in form to the term in the exact equation (Eq. (1)) that includes the gradients of mean pressure; specifically, the term that involves the product of the Reynolds stresses and the mean pressure gradient. The remaining terms either include gradients of temperature and velocity which are not present in the exact equation, or, for dimensional consistency, would require the introduction of a dependence on the temperature variance which is also absent from the exact equation. It is for this reason that it is argued here that the term involving the Reynolds stresses should alone be included in the model for $\overline{u_i t}$. After inclusion of the terms from the proposal of Younis et al. [19], the complete model now reads:

$$\begin{aligned}-\overline{u_i t} = {} & C_1\frac{k^2}{\epsilon}\frac{\partial T}{\partial x_i} + C_2\frac{k}{\epsilon}\left(\overline{u_i u_j}\frac{\partial T}{\partial x_j} - C_5\frac{1}{\rho c_p}\overline{u_i u_j}\frac{\partial P}{\partial x_j}\right) \\ & + C_3\frac{k^3}{\epsilon^2}\frac{\partial U_i}{\partial x_j}\frac{\partial T}{\partial x_j} + C_4\frac{k^2}{\epsilon^2}\left(\overline{u_i u_k}\frac{\partial U_j}{\partial x_k} + \overline{u_j u_k}\frac{\partial U_i}{\partial x_k}\right)\frac{\partial T}{\partial x_j}.\end{aligned} \tag{4}$$

It is worth noting that the additional term, being independent of the temperature gradients, implies that in an initially isothermal turbulent flow, such gradients can be generated by the application of pressure gradients.

The model given by Eq. (4) bears some similarity to an earlier model that was proposed by Deissler and Perlmutter [20] based on the theory of turbulent volume work in a pressure gradient. By utilizing certain empirical analogies with atmospheric processes, they proposed that the pressure gradient term should be included in the model for turbulent fluxes in the form:

$$-\overline{u_i t} = k_t\left(\frac{\partial T}{\partial x_i} - \frac{1}{\rho c_p}\frac{\partial P}{\partial x_i}\right) \tag{5}$$

where k_t is an eddy diffusivity. Their analytical solutions for the temperature distribution in a Ranque-Hilsch tube showed a static temperature distribution corresponding to an adiabatic change of state over the radial pressure distribution. The minimum value of static temperature was predicted to occur on the tube axis, in good agreement with experiments. The model of Eq. (4) can thus be considered a generalization of the isotropic model of Deissler and Perlmutter [20] via the presence of $\overline{u_i u_j}$ that brings about the consistency with the exact equation for the heat fluxes. The new model also provides a convincing explanation for the need for the explicit inclusion of a dependence on the gradients of mean pressure.

The complete model of Eq. (4) contains a number of coefficients that need to be determined. Of those, the coefficient of the original model of Younis et al. [19] that were determined by reference to results from Direct Numerical Simulations of some fundamental heated flows remain unchanged, viz. $C_1 = -0.0455, C_2 = 0.373, C_3 = -0.00373, C_4 = -0.0235$. This is logical, because in the absence of a strong pressure gradients, the new model should revert to its original form.

In determining the new coefficient (C_5), consideration must be given to the fact that the pressure gradient term must be balanced by the other terms in the model in such a way as to maintain the correct asymptotic behavior in conditions of strong pressure gradients and turbulence. This requirement can be seen when examining the physical process underlying the heat transfer processes in these conditions.

Briefly, turbulent eddies transport small amounts of fluid counter to the local pressure gradient. When moving along the pressure gradient into an area with higher pressure, these fluid volumes are compressed and volume work is done leading to rise in fluid temperature. In their final position the temperature is equalized to the new environment due to heat conduction. In strong turbulence this mechanism is much stronger than heat conduction and turbulent heat transport due to the temperature gradient, it results in a temperature distribution that looks like an adiabatic change of state. A temperature difference that is larger than the one corresponding to an adiabatic distribution is physically impossible. This has implications for the value of C_5. When the temperature distribution is similar to an adiabatic change of state compared to the pressure distribution, the influence of the pressure term, which is in part determined by C_5, has to be equal or smaller than the influence of the terms depending on the component of the temperature gradient, which is parallel to the pressure gradient.

To assess the relative importance of the terms that are functions of the gradients of temperature and pressure in isolation, we consider the case of flow in the x-direction, with velocity component U and a pressure gradient $\partial P/\partial x$. To balance the internal heat transfer due to the pressure gradient, the only relevant gradient of temperature is $\partial T/\partial x$. Under these circumstances, the model of Eq. (4) reduces to:

$$\begin{aligned}0 = {} & C_1\frac{k^2}{\epsilon}\frac{\partial T}{\partial x} + C_2\frac{k}{\epsilon}\left(\overline{u^2}\frac{\partial T}{\partial x} - C_5\frac{1}{\rho c_p}\overline{u^2}\frac{\partial P}{\partial x}\right) + C_3\frac{k^3}{\epsilon^2}\frac{\partial U}{\partial x}\frac{\partial T}{\partial x} \\ & + C_4\frac{k^2}{\epsilon^2}\left(\overline{u^2}\frac{\partial U}{\partial x} + \overline{u^2}\frac{\partial U}{\partial x}\right)\frac{\partial T}{\partial x}.\end{aligned} \tag{6}$$

It is immediately apparent that the terms $\overline{u^2}\partial T/\partial x$ and $C_5\frac{1}{\rho c_p}\overline{u^2}\partial P/\partial x$ are very similar in form. Considering the velocity

distribution in a vortex in Eq. (6), the terms containing C_3 and C_4 are much smaller than the term containing C_2, as the included velocity gradient $\partial U/\partial x$ becomes small (in the geometrical point that is discussed, the velocity component U is equal to the radial velocity. This is always almost equal to zero). Moreover, the term containing C_1 is of minor importance being much smaller than the term containing C_2.

When the heat transport is accomplished by fluid particles that are moving along a pressure gradient and work is done, they can maximally change their temperature according to an isentropic change of state. Thus, due to turbulence in a pressure gradient, the static temperature changes in its limit to a distribution adapting an adiabatic change of state compared to the pressure distribution. In this case the turbulent heat flux has to tend to zero, when neglecting heat conduction and convection. With this assumptions only the term belonging to the coefficient C_2 is able to balance the pressure term resulting in the following equilibrium:

$$0 = C_2 \frac{k}{\epsilon}\left(\overline{u^2}\frac{\partial T}{\partial x} - C_5 \frac{1}{\rho c_p}\overline{u^2}\frac{\partial P}{\partial x}\right) \tag{7}$$

$$\frac{\partial T}{\partial x} = \frac{C_5}{\rho c_p}\frac{\partial P}{\partial x}. \tag{8}$$

Integrating this equation results in

$$\frac{T}{T_0} = \left(\frac{P}{P_0}\right)^{\frac{\kappa-1}{\kappa}C_5}. \tag{9}$$

For an ideal gas with $C_5 = 1$ an isentropic change of state is obtained. The fact that turbulent particles move adiabatically in radial direction has also been noted by Deissler and Perlmutter [20].

Beside this consideration, the coefficient C_5 has also been determined out of the comparison of temperature calculations and measurements in the vortex chamber, which are presented in the next section. This results in the same value for C_5 as the one given above.

3. Experiments in a swirl chamber

3.1. Geometry

The flow in a swirl chamber provides an ideal manifestation of thermal energy separation by swirl as the geometry is fairly simple and the effect can be studied in isolation of other phenomena. In the present swirl chamber, which is depicted in Fig. 2, air is introduced via two tangential slots into a round tube with diameter $D = 50$ mm and length of 1 m. The slots themselves have a length $l = 0.66D$ and a width of $b = 0.1D$. The outlet from the tube is open and the pressure there is atmospheric. The tube walls are assumed to be adiabatic and the inlet temperature was maintained at a constant value of $T_E = 300$ K.

The strength of swirl is generally quantified by the swirl number i.e. by the ratio of the flux of tangential momentum I_Θ to that of axial momentum I_x:

$$S = \frac{I_\Theta}{RI_x} = \frac{\int_{r=0}^{R}\rho WU 2\pi r^2 dr}{R\int_{r=0}^{R}\rho U^2 2\pi r dr}. \tag{10}$$

where R is the pipe radius, r is the radial coordinate, U is the axial component of velocity and W the tangential velocity. For the flow inside a Ranque-Hilsch tube, the axial flow is bi-directional in the sense that the flows in the central core and the periphery move in opposite directions and thus the swirl number as defined in Eq. (10) would not be an appropriate indicator of the strength of swirl at a given streamwise section. At inlet to the swirl chamber, however, the axial flow is uniformly directed across the entire section and hence the swirl number as defined in Eq. (10) is a meaningful indicator of the strength of swirl at that location. This being the case, the inlet swirl number in the experiments is obtained as $S_I = 5.30$.

The Reynolds number is defined with the mean axial velocity of the flow U_0 and the tube diameter

$$Re_D = \frac{U_0 D}{\nu} = \frac{4\dot{m}}{\rho\pi D\nu}. \tag{11}$$

In the present experiment, the mean axial velocity was $U_0 = 6.18$ m/s and $Re_D = 20,000$.

3.2. Instrumentation

A schematic representation of the test rig used for the present experiments is shown in Fig. 3. Air entered the test section through a conical inlet where the mass flow has been measured using a laminar flow element (TetraTec LMF 50MC02-02-FS). According to the manufacturer, this mass flow element is accurate to within 0.15% of the actual value in the range 300–2400 l/min. From the mass flow element, the flow passed through a plenum chamber followed by a honeycomb flow straightener before entering the swirl chamber via the tangential slots. Downstream of the swirl chamber, the flow passed through a 500 mm long tube leading to a second plenum. The tube was made out of Plexiglass with a wall thickness of 20 mm. Thus the outer wall can be considered to be adiabatic. From there the air was sucked by a vacuum pump. In the PIV experiments, small oil droplets where injected directly after the first plenum.

Measurement of temperature was with thermocouples (type K, Omega 5SCTT-KI-40-2 M) with a manufacturer quoted accuracy of 0.3 K and a response time of 0.02 s at 18 m/s air speed. The voltage of the thermocouples was measured with an Agilent 34830A analyzer with external temperature reference. To measure the radial profile of fluid temperature, the test rig was equipped with a traversing mechanism that spanned the entire range. The wall

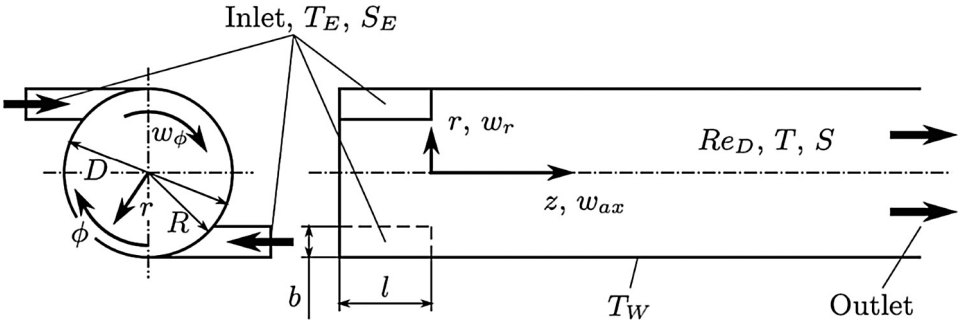

Fig. 2. Geometry of a swirl chamber.

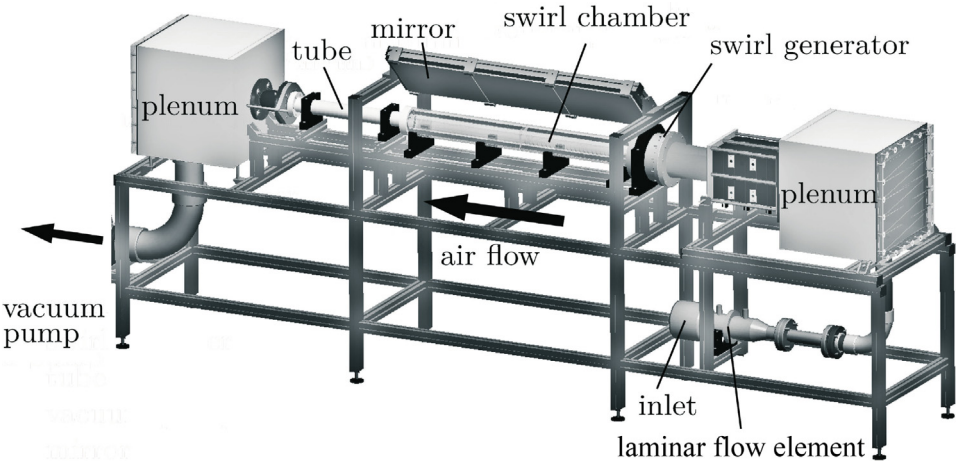

Fig. 3. Setup of the experimental test rig.

temperature T_W was measured using ten thermocouples that were placed directly below the surface at different axial positions. Measurement of velocity was by using a PIV system (Lavision). The air flow was seeded with small oil droplets with a diameter of about 0.25 μm. The oil droplets were generated using a Topas ATM210 aerosol generator which, according to the manufacturer, yields particle concentrations of the order of 10^8 particles/cm^3. The Stokes number, with the fluid time scale based on rotation of the main vortex, turns out to be approximately 1.8×10^{-4} – a value that is sufficiently small for the oil droplets to follow the air flow. A two-dimensional plane was illuminated twice by a laser sheet with a very short time delay. Each time an image was captured with a camera orientated perpendicularly to the laser sheet. The resolution of the camera is 900 pixels per tube diameter. The local velocities were deduced from the shift of the oil droplets between the two images. To do so, cross correlations between corresponding interrogation windows of 16×16 pixels of the two pictures have been calculated. The time delay between two laser flashes was chosen in a way that the fastest oil droplets have been shifted by 5 pixels. The shift of the oil droplets could be detected by the PIV system with an accuracy of 0.1 pixels resulting of an measurement error of 2% of the highest velocity in this section. The velocity field in each tube section is the result of the averaged value of 200 single measurements.

4. Results and discussion

4.1. Computational details

The computations were performed using the compressible flow form of the Ansys CFX (v. 11sp1) software in which the governing equations are discretized by second-order accurate finite-volume methodology. The unknown Reynolds stresses were obtained using an explicit algebraic Reynolds stress model [21,22] incorporating the modification proposed by Wallin and Johansson [23] to account for streamline curvature. This combination of closures was found to yield sufficiently accurate predictions of the Reynolds stresses for input into the model for the turbulent heat fluxes. Implementation of the latter into the computations software was fairly straightforward and was accomplished via user defined subroutines. For comparison, a model with a constant turbulent Prandtl number $Pr_t = 0.9$ was also used. The assumption that the flow in the swirl chamber is axi-symmetric, which is often made in the calculation of these flows, was not invoked here. Instead, fully three dimensional computations were performed on a number of structured O-grids with varying number of cells, with the finest consisting of 1.5 million non-uniformly distributed active cells. The first grid point near the wall was placed at a distance $y_1^+ < 1$ (where $y^+ = y u_\tau / \nu$ with y being the normal distance to the wall, and u_τ is the shear velocity). This was done to ensure that the computations accurately captured the steep temperature gradients that occurred there. The refinement factor for the thickness of the grid cells from the wall is 1.20.

The sensitivity of the computed results to grid density and distribution was assessed using the Grid Convergence Index (GCI) method. After calculating the numerical solution on three grids with different number of cells, an asymptotic solution on a grid with an infinite number of cells is estimated by Richardson extrapolation. This allows for the error between the actual numerical solution and the asymptotic solution to be estimated. In the present study (with $S_E = 2.95$ and $Re_D = 20,000$), the number of cells of the used grid was bisected twice. The estimated mean error of the axial velocity is 0.76%, for the circumferential velocity 1.28% and for the temperature 0.26%.

4.2. Comparisons with measurements

The computed and measured cross-stream profiles of the axial component of velocity are compared in Fig. 4. The results are presented at three streamwise locations viz. $z/d = 6.2$, 9 and 15.5. As expected, the computational results are exactly symmetric around the centerline. The adverse pressure gradients set-up by the swirling motion leads to the establishment of a central region of reversed flow with the velocity maxima now occurring closer to the outer walls. The correspondence with the measured profiles are generally good considering the inevitable uncertainty in the latter which is estimated at around 5% at the centerline.

The computed and measured circumferential velocity at four streamwise locations along the vortex chamber are compared in Fig. 5. The circumferential velocity was non-dimensionalized using the average streamwise velocity. As can be seen from the figure, and as suggested by Marsik et al. [24], the flow field in the vortex chamber can be viewed as a combination of a Rankine vortex and a wall boundary layer. In the core of the vortex the fluid rotates like a solid body with constant angular velocity. The circumferential velocity increases linearly with the radius. Around the viscous core there is a transition area, where the shape of the flow changes to the outer flow region with an almost potential like vortex. Near the wall, the existence of a viscous boundary layer is apparent. The circumferential velocity decreases over the chamber length

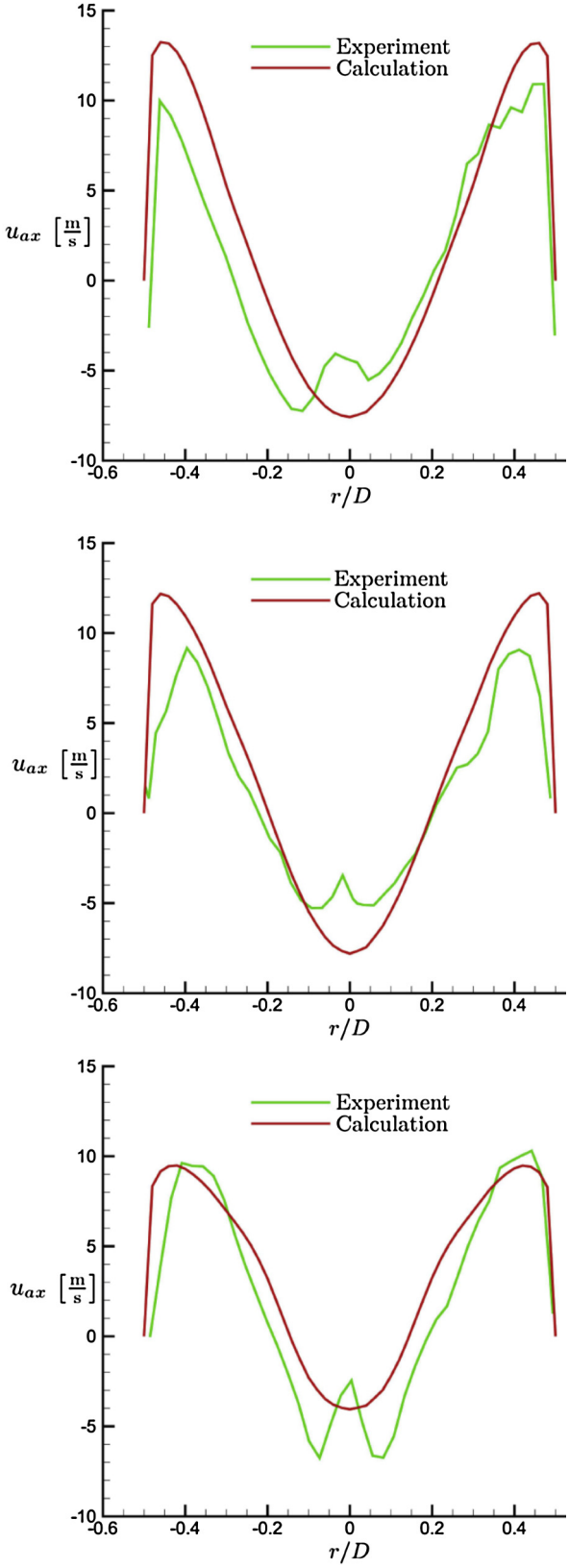

Fig. 4. Predicted and measured axial velocity $S_l = 5.30, Re_D = 20,000$. From top: $z/D = 6.2$, 9.0, 15.5.

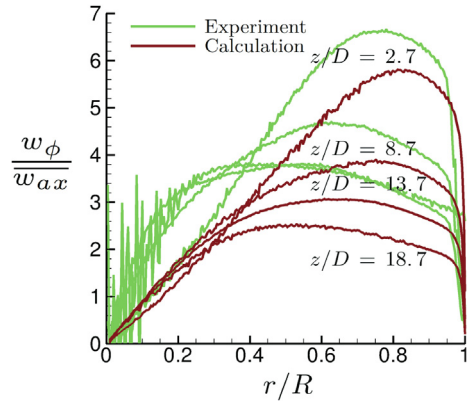

Fig. 5. Predicted and measured circumferential velocity $S_l = 5.30, Re_D = 20,000$.

as the swirl dissipates. The viscous core is most pronounced in the front part of the chamber ($z/D = 2.7$). Its diameter decreases over the tube length and the position of the maximal velocity in each cross section moves closer to the axis. Near the entrance to the chamber, the calculated and measured velocity profiles agree fairly well. The streamwise development of the vortex core does not appear to be predicted very accurately, as the angular velocity remains constant, whereas in the measurements the angular velocity increases, and the diameter of the viscous core decreases faster as in the numerical computation. Outside the viscous core, in the region of the potential vortex, the agreement between numerical calculations and experiments is far better. Experimental errors in PIV measurements, evident here in the high-frequency oscillations near the core, are estimated at 20%.

The predicted and measured contours of the axial velocity are compared in Fig. 6. The swirl in the vortex chamber is sufficiently strong so as to cause vortex breakdown. This is evident by the presence of forward streamwise flow near the wall, and reversed flow in the core over the whole length of the chamber. In obtaining the measurement of axial velocity near the entrance to the chamber, the circumferential velocity there was very high to the extent that the oil droplets left the laser sheet too quickly so no accurate measurements of the axial velocity were possible there. In Fig. 6 this area is seen shaded in grey in order to make clear that the measurements there are subject to large uncertainty. In the downstream end of the chamber, only a few oil droplets remained within the middle of the core of the vortex. It is thus the case that the low velocity within the axial backflow in this region was also subject to high experimental uncertainty.

The computed contours of static temperature are presented in Fig. 7. It should here again be noted that the outer wall of the tube is adiabatic. The results were obtained with the new model for heat fluxes (Eq. (4)) with $C_5 = 1.0$. The swirl-induced temperature separation can clearly be seen there. The static temperature is minimum in the core of the vortex, especially at entrance to the chamber where the swirl is strongest. Further downstream, the degree of temperature separation is reduced as the swirl weakens and with it the radial gradients of static pressure. It is interesting to note that the predicted mean temperature in a cross section at entrance to the chamber is lower than near the exit. At first sight, this would appear to be in violation of the conservation of energy. However, as there is a large area of axial backflow in the core of the vortex, it was confirmed that the mass flow averaged transport of energy at all cross sections of the chamber remained constant.

The predicted and measured cross-stream profiles of static temperature (presented as the ratio T_c/T_W of the centerline to wall temperature) are shown in Fig. 8. Plotted there are results obtained with the new model with three different values for the coefficient C_5 to check the sensitivity of the results to this coefficient. Also plotted there are results obtained using the conventional Fourier's law with constant turbulent Prandtl number. With the coefficient

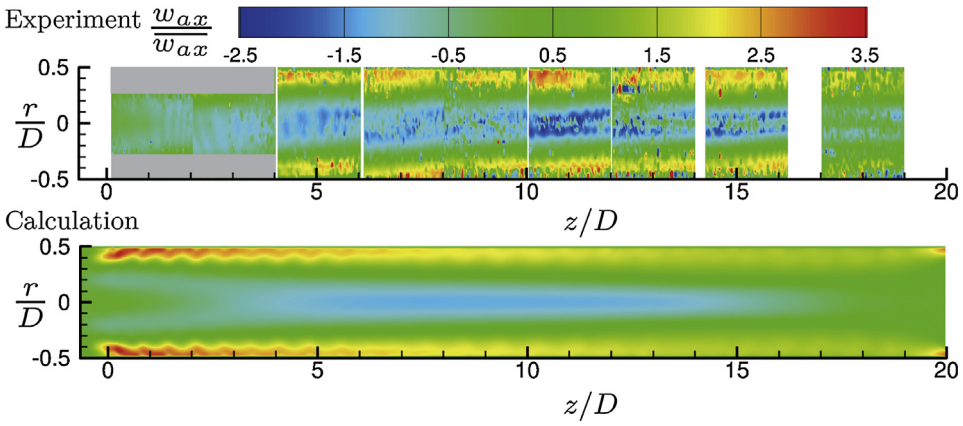

Fig. 6. Predicted and measured contours of axial velocity $S_l = 5.30, Re_D = 20,000$.

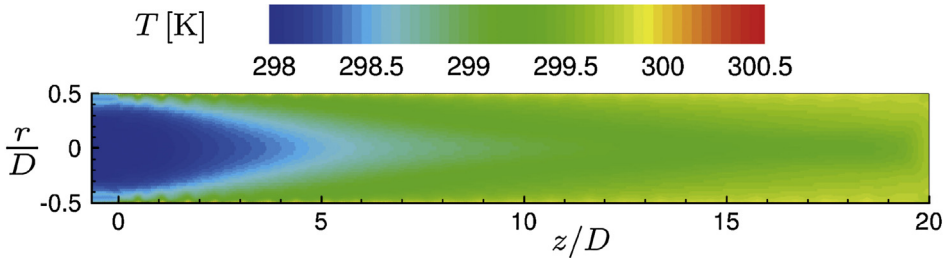

Fig. 7. Predicted contours of static temperature $S_l = 5.30, Re_D = 20,000$.

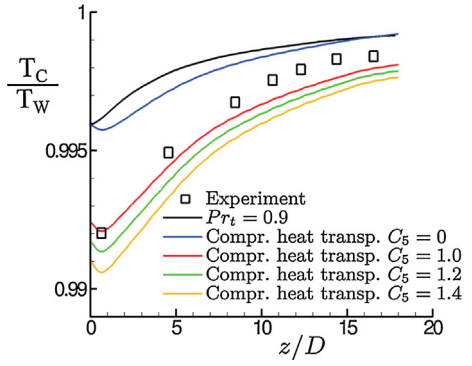

Fig. 8. Predicted and measured streamwise variation of static temperature along the axis, $S_l = 5.30, Re_D = 20,000$.

$C_5 = 1.0$, the new model provides the closest agreement between the numerical predictions and the experiments. This confirms the validity of the arguments presented earlier in support of this value. In the downstream part of the chamber, the centerline temperature is somewhat underestimated. That is caused by the deviation of the circumferential velocity shown in Fig. 5. The results obtained with Fourier's law show that the temperature separation is drastically underestimated. At entrance to the chamber, the static temperature is slightly reduced due to the dynamic part of energy, whereas the wall temperature is predicted as being equal to the total temperature.

The predicted radial variation of axial and tangential velocities and of pressure at the streamwise position $z/D = 0.32$ are presented in Fig. 9. As the flow is dominated by vortex breakdown, the axial velocity (u_{ax}) is positive near the wall and negative in the core of the vortex. The circumferential velocity (u_ϕ) shows a

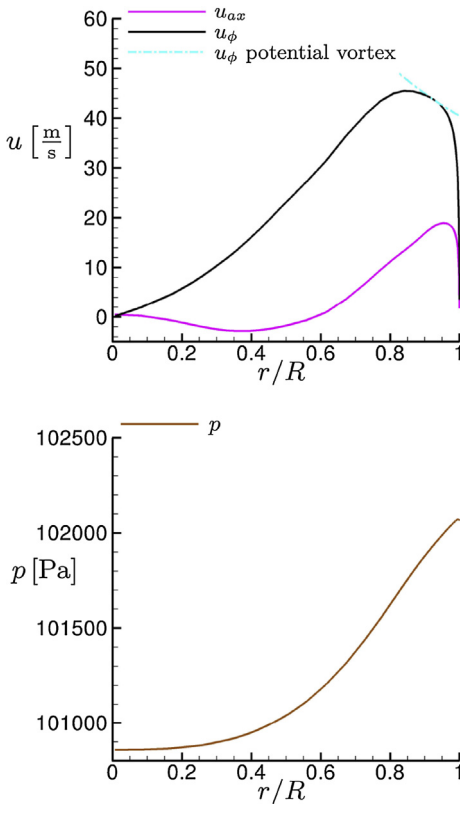

Fig. 9. Radial distribution of velocity and pressure for $z/D = 0.32, S_l = 5.30, Re_D = 20,000$.

pronounced region with a solid body velocity profile and a boundary layer near the wall. Due to centrifugal forces, the pressure increases over the radius.

Fig. 10 shows the predicted and measured radial distribution of temperature, also at $z/D = 0.32$. Both the static and total temperatures are shown. As expected, the swirl-induced temperature separation leads to pronounced increase in static temperature with increasing radial distance from the centerline.

Concerning the temperature measurements, in experiments such as this one where thermocouples are used, a difficulty arises since due to the boundary layer effects on the surface of the thermocouples, the temperature values that are measured do not exactly represent the free-stream temperature but a value in between T and T_{total}. This is also the case for all other temperature probes and is usually accounted for by the introduction of a recovery factor f:

$$T_{measured} = T + f\frac{V^2}{2c_p} \tag{12}$$

In the above, by setting $f = 0$, the static temperature T is obtained, while setting $f = 1$ yields the total temperature T_{total}. In this study, the recovery factor was set to $f = 0.9$ which is appropriate for the turbulent flow of air, where the recovery factor scales as $\sqrt[3]{Pr}$. Therefore, the measured temperature is 10% of the dynamic part of the temperature below total temperature. In order to properly compare the measured and simulated temperatures, the numerical results for T were post-processed according to Eq. (12) with $f = 0.9$. The result is shown in Fig. 9 where it can be seen to closely match the measured total temperature T_{total}.

According to the arguments on swirl-induced temperature separation presented earlier, the static temperature should increase with the pressure like an isentropic change of state. This behavior is plotted in Fig. 10 where it is labeled ($T/T_W theory$). The result correlates well with the numerically calculated static temperature distribution. In the viscous boundary layer, the static temperature increases towards the total temperature. In the core of the vortex chamber, with the flow being in almost solid body rotation, there occurs a significant change in total temperature. This is the most important region for the swirl-induced temperature separation. In the area with an almost potential like vortex flow, there is only a smaller increase of total temperature. This corresponds well with the theory. It can be shown analytically that, in a potential vortex, the total temperature would be constant when defining the static temperature to show an adiabatic change of state compared to the pressure profile and assuming an ideal gas, whereas in a vortex the shape of a solid body rotation total temperature will increase with the radius.

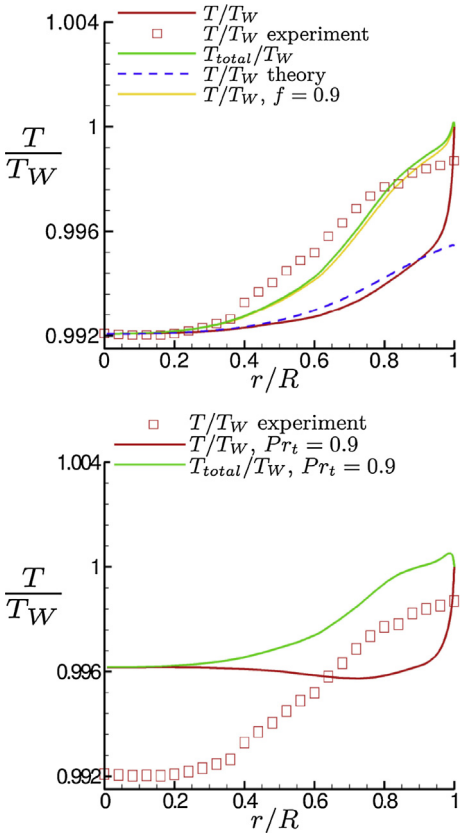

Fig. 10. Radial distribution of temperature for $z/D = 0.32, S_l = 5.30, Re_D = 20,000$.

Fig. 10 also shows calculations obtained by using Fourier's law with a constant turbulent Prandtl number of $Pr_t = 0.9$. In contrast with the results obtained with the new heat-flux model, these fail to capture the temperature change especially in the tube center. Indeed the static temperature turns out to be almost constant over the radius with a very slight increase towards the axis. There is a small separation of total temperature due to the higher velocity in the outer parts of the flow. This is the same behavior that can be expected to occur in incompressible fluids like water, and is a further demonstration of the important role that compressibility effects play in swirl-induced temperature separation.

5. Conclusions

The results presented in this paper demonstrate the importance of accounting for the effects of pressure gradients in the prediction of swirl-induced thermal energy separation. Conventional models for the turbulent heat fluxes, exemplified by Fourier's law with constant turbulent Prandtl number, do not take these effects into account. That the effects of pressure gradients should appear explicitly in a model for the turbulent scalar fluxes is apparent from the appearance of these gradients in the exact equations governing the conservation of these fluxes. An algebraic model for the turbulent heat fluxes was thus developed to explicitly include the pressure-gradient effects. The model is based on an earlier version that was limited to incompressible flows in which the pressure-gradient terms were insignificant. The new model introduced a single new coefficient whose value was set to unity based on theoretical consideration derived from analysis of an idealized swirling flow. Verification of this model was performed via comparisons with experimental data obtained in a swirl chamber. It was found that at the entry region to the chamber, where the swirl effects are most pronounced, the predictions obtained with the new model matched quite closely the experimental results to within the estimated accuracy in the latter. It should be noted that the temperature variations in the experiment were not very large and hence the close agreement obtained here does not necessarily mean that the model would be equally successful in predicting the Ranque-Hilsch regime of parameters where the temperature differences are much larger. In general, where the velocity field was accurately predicted, so was the temperature distribution obtained with the new model. The swirl-induced temperature separation was clearly evident with a cold vortex core and a temperature distribution that looks almost like an adiabatic change of state compared to the pressure. In contrast, the results obtained with Fourier's law and a constant Prandtl number were seriously in error in that the predicted static temperature profile was almost flat across the swirl vortex.

Conflict of interest

The authors declare that there is no conflict of interest.

Acknowledgments

This work was funded by the German Federal Ministry of Economic Affairs and Energy, BMWi and Rolls-Royce under project LuFo4 RobusTurb. We are indebted to the anonymous reviewer who drew our attention to the reference from which the exact compressible flow equation for the turbulent heat fluxes was obtained.

References

[1] G.J. Ranque, Experiences sur la detente giratoire avec simultanes d'un echappement d'air chaud et d'un enchapement d'air froid, J. Phys. Radium 4 (1933) 112–114.
[2] R. Hilsch, The use of the expansion of gas in a centrifugal field as cooling processes, Rev. Sci. Instr. 18 (1947) 108–113.
[3] S. Eiamsaard, P. Promvonge, Numerical investigation of the thermal separation in a Ranque-Hilsch vortex tube, Int. J. Heat Mass Transf. 50 (2007) 821–832.
[4] U. Behera, P.J. Paul, K. Dinesh, S. Jacob, Numerical investigations in flow behaviour and energy separation in Ranque-Hilsch vortex tube, Int. J. Heat Mass Transf. 51 (2008) 6077–6089.
[5] M. Kurosaka, Acoustic streaming in swirling flow and the Ranque-Hilsch vortex-tube effect, J. Fluid Mech. 124 (1982) 139–172.
[6] A.F. Gutsol, The Ranque effect. Physics Uspekhi, Russ. Acad. Sci. 40 (1997) 639–658.
[7] E.R.G. Eckert, Energy separation in fluid streams, Int. Commun. Heat Mass Transf. 13 (1986) 127–143.
[8] B.A. Shannak, Temperature separation and friction losses in vortex tube, Heat Mass Transf. 40 (2004) 779–785.
[9] S.A. Piralishvili, A.A. Fuzeeva, Hydraulic characteristics of Ranque-Hilsch energy separator, High Temp. 43 (2005) 900–907.
[10] K. Dincer, S. Baskaya, B.Z. Uysal, Experimental investigations of the effects of length to diameter ratio and nozzle number on the performance of counter flow Ranque-Hilsch vortex tubes, Heat Mass Transf. 44 (2008) 367–373.
[11] R.T. Balmer, Pressure-driven Ranque-Hilsch temperature separation in liquids, J. Fluids Eng. 110 (1988) 161–164.
[12] J.G. Polihronov, A.G. Straatman, Thermodynamics of angular propulsion in fluids, Phys. Rev. Lett. 109 (2012) 054504 1–054504 4.
[13] H.R. Thakare, A. Monde, A.D. Parekh, Experimental, computational and optimization studies of temperature separation and flow physics of vortex tubes: a review, Renew. Sustain. Energy Rev. 52 (2015) 1043–1071.
[14] T. Karthikeya Sharma, G.A.P. Rao, K.M. Murthy, Numerical analysis of a vortex tube: a review, Arch. Comput. Methods Eng. 24 (2017) 251–280.
[15] T. Farouk, B. Farouk, Large eddy simulations of the flow field and temperature separation in the Ranque-Hilsch vortex tube, Int. J. Heat Mass Transf. 50 (2007) 4724–4735.
[16] C. LE Ribault, R. Friedrich, Investigation of transport equations for turbulent heat fluxes in compressible flows, Int. J. Heat Mass Transf. 40 (1997) 2721–2738.
[17] G.K. Batchelor, Diffusion in a field of homogeneous turbulence, Aust. J. Sci. Res. A2 (1949) 437–450.
[18] G.F. Smith, Constitutive Equations for Anisotropic and Isotropic Materials, North–Holland, 1994.
[19] B.A. Younis, C.G. Speziale, T.T. Clark, A rational model for the turbulent scalar fluxes, Proc. Roy. Soc. A 461 (2005) 575–594.
[20] R.G. Deissler, M. Perlmutter, Analysis of the flow and energy separation in a turbulent vortex, Int. J. Heat Mass Transf. 1 (1960) 173–191.
[21] S. Wallin, A.V. Johansson, An explicit algebraic Reynolds stress model for incompressible and compressible turbulent flows, J. Fluid Mech. 403 (2000) 89–132.
[22] A. Hellsten, New advanced k-omega turbulence model for hight-lift aerodynamics, AIAA J. 43 (2005) 1857–1869.
[23] S. Wallin, A.V. Johansson, Modelling streamline curvature effects in explicit algebraic Reynolds stress turbulence models, Int. J. Heat Fluid Flow 23 (2002) 721–730.
[24] F. Marsik, B. Kobiela, P. Novotny, B. Weigand, Thermodynamics analysis and experimental investigation of swirl tube flow, in: 21st Int.l Symp. on Transport Phenomena, Kaohsiung City – Taiwan, 2010.